ceramics

MDPI

Article

Electrical Behavior of Electric Field-Assisted Pressureless Sintered Ceria-20 mol% Samaria

Shirley L. Reis [1,*], Sabrina G.M. Carvalho [1], Eliana N.S. Muccillo [1] and Reginaldo Muccillo [1,2]

[1] Energy and Nuclear Research Institute, São Paulo 05508-170, Brazil; sabrina.carvalho@usp.br (S.G.M.C.); enavarro@usp.br (E.N.S.M.); muccillo@usp.br (R.M.)
[2] Federal University of ABC, Santo André 09210-580, Brazil
* Correspondence: shirley.reis@usp.br; Tel.: +55-11-31339203

Received: 12 April 2019; Accepted: 20 May 2019; Published: 1 June 2019

Abstract: CeO_2:20 mol% Sm_2O_3 green ceramic pellets were sintered conventionally at 1500 °C/2 h and flash sintered by applying a 200 V cm^{-1} electric field at 800 °C, 1000 °C and 1200 °C. The thickness shrinkage of the pellets was followed bythe specimen being positioned inside a dilatometer adapted with platinum electrodes and terminal leads connected to a power supply for application of the electric voltage. The microstructure of the surfaces of the sintered samples were observed in a scanning electron microscope. The electrical properties were evaluated by the impedance spectroscopy technique in the 5 Hz–13 MHz frequency range from 210 °C to 280 °C. The main results show that (i) the final shrinkage level is nearly independent of the temperature when the electric field is applied and slightly better than that of the 1500 °C sintered pellet, and (ii) the bulk conductivity of the sample flash sintered at 1200 °C is similar to that of the sample sintered at 1500 °C. The availability of a pathway for the electric current pulse derived from the applied electric field is proposed as the reason for the achieved shrinkages. Scavenging of the grain boundaries by Joule heating is proposed as the reason for the improved oxide ion bulk conductivity.

Keywords: samaria-doped ceria; flash sintering; dilatometry; impedance spectroscopy

1. Introduction

1.1. Flash Sintering

Sintering a ceramic body by applying an electric field without application of pressure at a temperature below the temperature usually used for sintering is a technique that has been applied since it was first proposed in 2010 [1]. Several review papers have shown the application of this technique to electroceramics, insulators, semiconductors and mainly, ionic conductors [2–6]. Most of the studied ionic conductors are either 3 mol% or 8 mol% stabilized zirconia [1,7–25]. The advantage of performing flash sintering experiments on those compounds is that besides having chemical stability, their properties have been widely studied for decades [26]. However, there are few reports on flash sintering ceria-based solid electrolytes [27–33].

1.2. Flash Sintering Ceria

Fully dense $Ce_{0.8}Gd_{0.2}O_{1.9}$ specimens have been sintered under DC electric fields with decreasing average grain size, and with increasing field and decreasing sintering temperature [27]. $Ce_{0.8}Gd_{0.2}O_{1.9}$, $Ce_{0.9}Gd_{0.1}O_{1.95}$ and $Ce_{0.8}Sm_{0.2}O_{1.9}$ were found to flash sinter at 554 °C, 635 °C and 667 °C, respectively, well below their conventional sintering temperatures [28]. Conventional and flash sintered nanosized 10 mol% Gd_2O_3-doped CeO_2 produced dense specimens with uniform submicrometric grains [29]. Tape cast $Ce_{0.9}Gd_{0.1}O_{1.95}$ has been reported to reach high densification if the limit of the current

density is appropriate, and particle size, porosity and homogeneity also played a role in the flash sintering results [30]. Gd- and Sm-doped ceria with Li and Co sintering aids were flash sintered to full density in short times at 700 °C, and achieved total ionic conductivity comparable to that obtained in samples conventionally sintered at 1500 °C [31]. Dense $Ce_{0.8}Sm_{0.2}O_{1.9}$ were obtained by flash sintering at low temperatures with DC electric fields, with the final density depending on the control of the electric current density. Moreover, temperature, density and particle size gradients were observed in sintered bodies, probably due to electrochemical effects (mass transfer) of the DC electric field [32]. Flash sintering is known to produce dense samples without any evident increase in average grain size at relatively low temperatures when compared to samples obtained by conventional sintering. The application of AC instead of DC electric fields in ionic conductors is preferable to avoid non-homogeneous distribution of grain sizes [22,33].

The main difference between the two oxide ion conductors, yttria-stabilized zirconia and gadolinia- or samaria-doped ceria is that even though ceria-based compounds have higher ionic conductivity than stabilized zirconias, their electron transport number is not null at high temperatures. That means that at usual flash occurring temperatures, oxide ions and electrons are the charge carriers in ceria compounds, while mainly oxide ions take part in the electrical conductivity of zirconia compounds [34].

For the first time, this study report the results of AC electric field-assisted (flash) pressureless sintering CeO_2: 20 mol% Sm_2O_3 green pellets at different temperatures with a fixed electric field and a current limit with fairly high density. Their electrical resistivity was evaluated by the impedance spectroscopy technique and compared to that of conventionally sintered samples. Moreover, scanning electron microscopy images were collected for estimation of average grain sizes and residual porosities.

2. Materials and Methods

The samaria-doped ceria, $(CeO_2)_{0.8}(Sm_2O_3)_{0.2}$ (SDC20), commercial ceramic powders with 36.1 $m^2\ g^{-1}$ surface area (Fuel Cell Materials, USA [35]), were uniaxially cold pressed into φ 5 mm and 5 mm thick cylindrical shapes at 65 MPa. The geometrical density was ~45% T.D. (T.D., theoretical density = 7.14 g cm^{-3}). The density of the sintered samples was evaluated by the Archimedes technique in a Mettler Toledo AG245 balance.

The pellets were sintered following two techniques: (a) heating to 1500 °C and cooling to room temperature in a vertical dilatometer (TA Dil 822, New Castle, DE, USA) with 10 °C min^{-1} heating and cooling rates; and (b) isothermal electric field-assisted pressureless sintering at 800 °C, 1000 °C and 1200 °C. Pellets were also sintered in air at 1500 °C/2 h in a Lindberg-Blue M furnace (Watertown, USA). For electric field-assisted sintering, the green pellet was positioned between two platinum electrodes inside a vertical dilatometer (Unitherm 1161, Anter, Pittsburgh, PA, USA) [11], with the electrodes being connected to a power supply (Pacific Power Source 118-ACX, Irvine, CA, USA) designed to apply AC voltages up to 150 V with frequency ranging from 15 to 1200 Hz and 20 A maximum limit current. The power supply operates in a current limit mode, changing the applied voltage to keep the preset electric current constant. Therefore, an electric power peak occurs to maintain the current limit, and then it changes to a nearly steady state; the frequency of the applied electric field was fixed at 1000 Hz [22].

After sintering, the samples were characterized by (i) apparent density measurements by the Archimedes technique, (ii) observation of polished surfaces by scanning electron microscopy, (iii) evaluation of the electrical resistivity by impedance spectroscopy, and (iv) structural phase analysis by X-ray diffraction.

The parallel surfaces of polished (diamond pastes, 15 μm to 1 μm) and thermally etched (100 °C below the sintering temperature) samples were observed in a scanning electron microscope (Inspect F50 FEG-SEM, FEI, Brno, Czech Republic).

Impedance spectroscopy measurements were performed in the 5 Hz–13 MHz frequency range in the 270–480 °C temperature range with 200 mV AC input bias in a HP 4192A impedance analyzer

connected to a HP 362 controller; silver was used as the electrode. The $[-Z''(\omega) \times Z'(\omega)]$ data were collected and analyzed with a special software [36].

3. Results

Figure 1 shows dilatometric curves of SDC20 green pellets from room temperature to 1500 °C with 26.4% final shrinkage, and with application of 200 V cm^{-1}, 1 kHz, 1.5 A limiting current, at 800 °C, 1000 °C and 1200 °C, all with 27.9% final shrinkage. The data were normalized to the initial thickness of the samples.

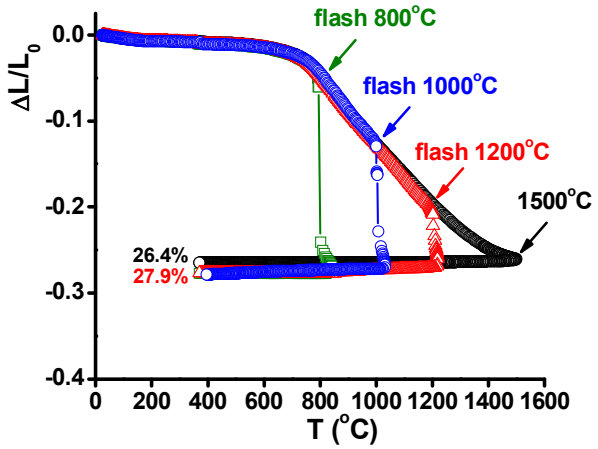

Figure 1. Dilatometric curves of $(CeO_2)_{0.8}(Sm_2O_3)_{0.2}$ with application of 200 V cm^{-1} at 800 °C, 1000 °C and 1200 °C for 5 min, limiting the electric current to 1.5 A. Also shown for the specimen conventionally sintered at 1500 °C.

The apparent densities (%T.D.) of the specimens flash sintered at 800 °C, 1000 °C and 1200 °C were 82%, 88% and 92%, respectively; the specimen conventionally sintered at 1500 °C achieved 96% T.D. Figure 2 shows X-ray diffraction results of the SDC20 specimens sintered at 1500 °C and with application of 200 V cm^{-1} during 5 min at 1200 °C. Both patterns are identical and correspond to the ICDD 28-792 file.

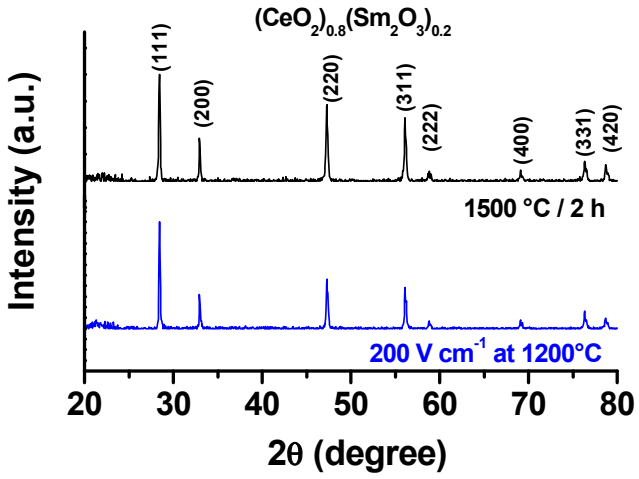

Figure 2. XRD patterns of $(CeO_2)_{0.8}(Sm_2O_3)_{0.2}$ sintered at 1500 °C/2 h and flash sintered with application of 200 V cm^{-1} at 1200 °C for 5 min.

Figure 3 shows scanning electron microscopy images of samples sintered at 1500 °C and flash sintered at 800 °C, 1000 °C and 1200 °C (Cf. Figure 1). The images were collected at the center of

parallel surfaces of the polished samples. The images are typical, and no noticeable difference was observed in different regions.

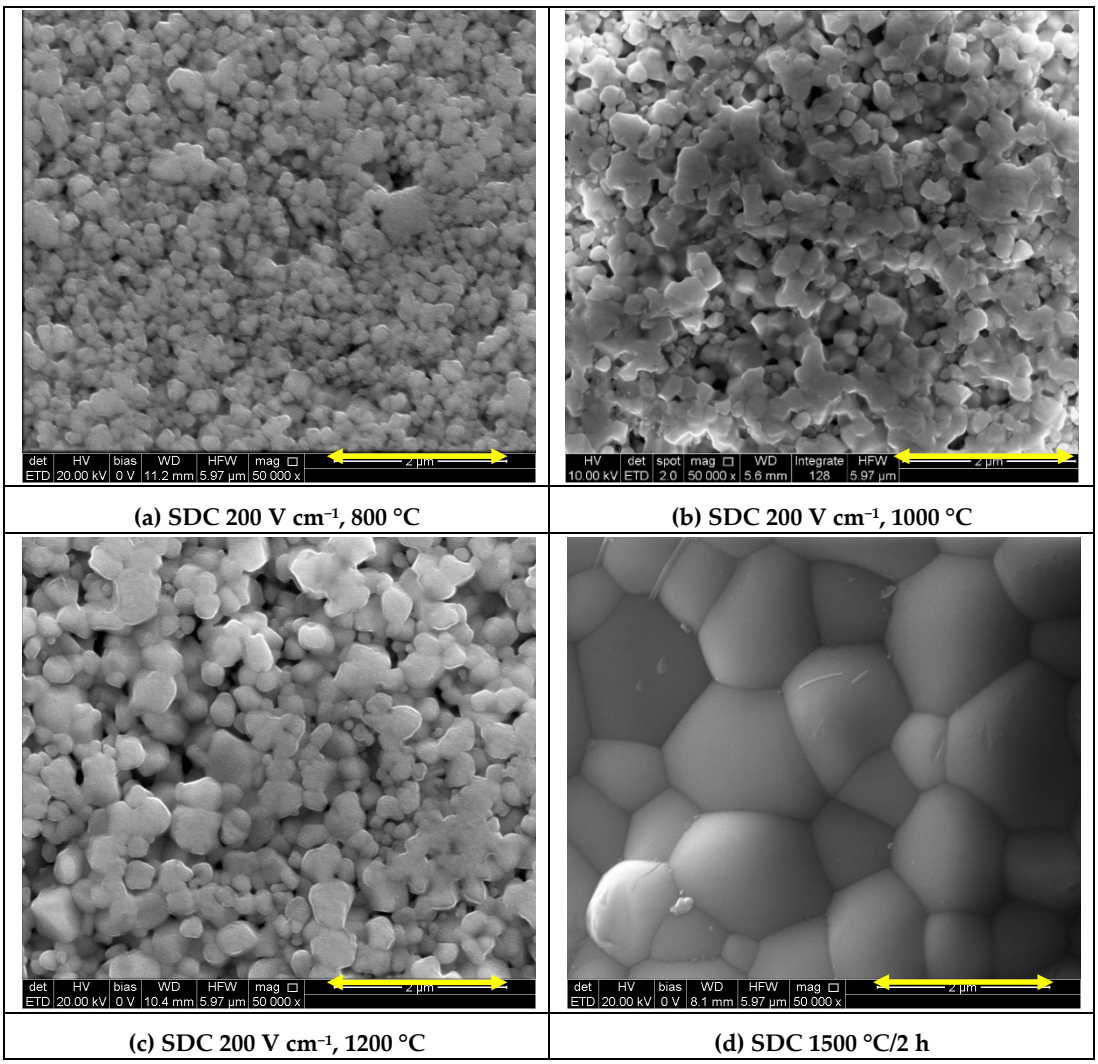

(a) SDC 200 V cm^{-1}, 800 °C | **(b) SDC 200 V cm^{-1}, 1000 °C**

(c) SDC 200 V cm^{-1}, 1200 °C | **(d) SDC 1500 °C/2 h**

Figure 3. Scanning electron microscopy micrographs of $(CeO_2)_{0.8}(Sm_2O_3)_{0.2}$ flash sintered for 5 min under 200 V cm^{-1} and 1.5 A limiting current at (**a**) 800 °C, (**b**) 1000 °C and (**c**) 1200 °C, and conventionally sintered at (**d**) 1500 °C/2 h; bar: 2 µm.

Figure 4 shows the $[-Z''(\omega) \times Z'(\omega)]$ impedance spectroscopy diagrams and the equivalent circuit of a sample sintered at 1500 °C/2 h and of the three samples sintered at 800 °C, 1000 °C and 1200 °C with application of 200 V cm^{-1} for 5 min[1], 1 kHz, limiting the electric current through the samples to 1.5 A. The diagrams show two main responses: one semicircle at high frequencies due to the intragranular (bulk) contribution to the resistivity, and another at intermediate frequencies due to the intergranular (grain boundaries and pores) contribution [37].

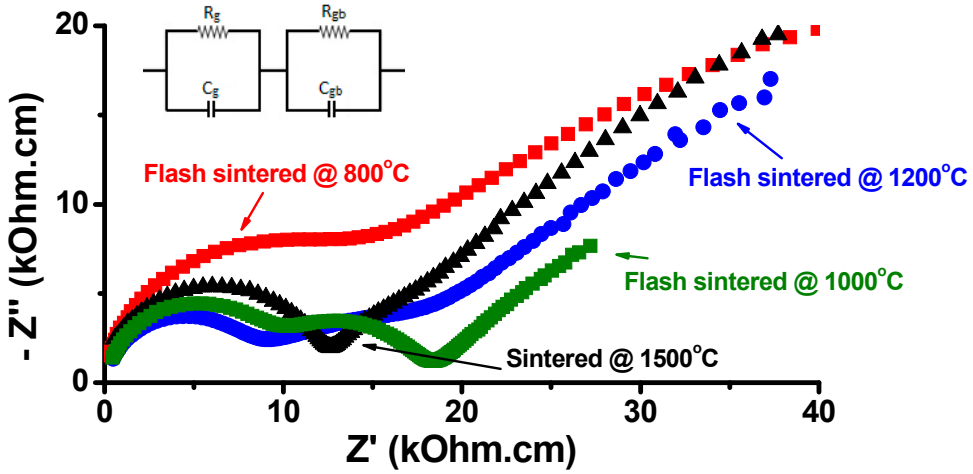

Figure 4. Impedance spectroscopy diagrams of $(CeO_2)_{0.8}(Sm_2O_3)_{0.2}$ flash sintered at 800 °C, 1000 °C and 1200 °C under 200 V cm^{-1}, 1 kHz, 1.5 A limiting current for 5 min, and conventionally sintered at 1500 °C/2 h. Temperature of measurement: 270 °C. Inset: equivalent circuits.

The Arrhenius plots of the intragranular (bulk) electrical conductivity measured at several temperatures in the 270–480 °C are shown in Figure 5. The data fitted well to straight lines, as expected. From the highest to the lowest conductivities, the sequence is: sample flash sintered at 1200 °C, flash sintered at 1000 °C, conventionally sintered at 1500 °C, flash sintered at 800 °C.

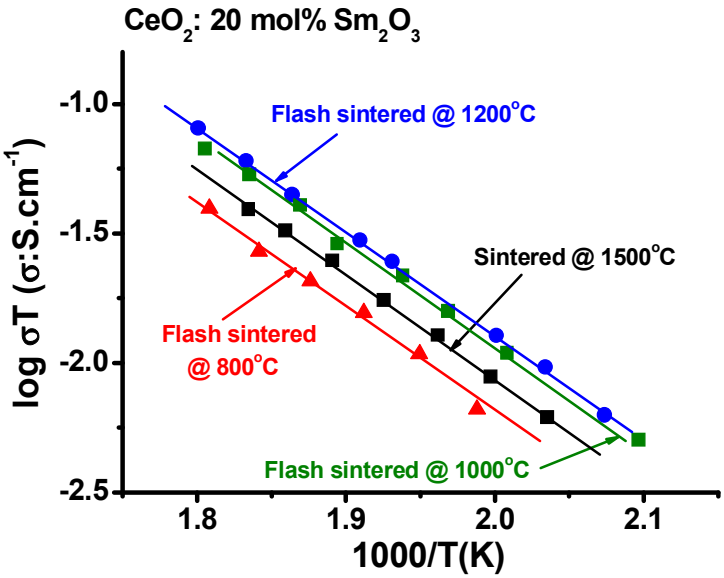

Figure 5. Arrhenius plots of the bulk electrical conductivity of $(CeO_2)_{0.8}(Sm_2O_3)_{0.2}$ flash sintered at 800 °C, 1000 °C and 1200 °C under 200 V cm^{-1}, 1 kHz, 1.5 A limiting current for 5 min, and conventionally sintered at 1500 °C/2 h.

4. Discussion

In the dilatometric curves of the $(CeO_2)_{0.8}(Sm_2O_3)_{0.2}$ ceramic samples, Figure 1, a 1.5% difference in the thickness shrinkage of the conventionally sintered pellet compared to the flash sintered pellets was measured. The electric field applied at 800 °C promotes a 21% thickness decrease while at 1200 °C that decrease is only 6.8%. This is due to the percolation of the electric current through the pellet, which is expected to be higher in samples with higher pore content, pores being considered the preferential pathway for the electric current. The Joule heating caused by the electric current increases the internal temperature of the sample enhancing the densification rate, achieving near full density.

The average grain sizes of the flash sintered $(CeO_2)_{0.8}(Sm_2O_3)_{0.2}$ samples, evaluated in the scanning electron microscopy images in Figure 3 are all in the submicron range and increase slightly for increasing flash sintering temperature: 0.28 μm, 0.34 μm and 0.69 μm in samples flash sintered at 800 °C, 1000 °C and 1200 °C, respectively. The sample conventionally sintered at 1500 °C, on the other hand, has larger average grain size (approximately 1.5 μm) as expected, and is apparently devoid of pores. Pores are visible in the flash sintered sample surfaces.

The impedance diagrams of the sintered $(CeO_2)_{0.8}(Sm_2O_3)_{0.2}$ ceramic samples (Figure 4), after deconvolution parametrized in frequency allows for evaluating the resistivities. The results show that increasing the temperature in which the electric field is applied promotes a decrease in the bulk resistivity: 15.3 Ohm·cm (800 °C), 10.8 Ohm·cm (1000 °C) and 9.5 Ohm·cm (1200 °C). The electrical resistivity of the sample sintered at 1500 °C was evaluated as 12.7 Ohm·cm. The relatively lower bulk resistivity of the flash sintered samples may be due to the diffusion of the samarium ions located at the space charge region back to the bulk due to the intense Joule heating caused by the electric current pulse [25]; that diffusion could promote an increase in the concentration of oxygen vacancy, which is the charge carrier of the electrical resistivity.

The Arrhenius plots of the bulk electrical conductivity of the $(CeO_2)_{0.8}(Sm_2O_3)_{0.2}$ ceramic samples (Figure 5) show parallel straight lines resulting from fitting the conductivity data after sintering either with the application of electric field at 800 °C, 1000 °C and 1200 °C or by heating to high temperature (1500 °C), indicating that the charge carrier is the same. From the slope of the line segment, taking into account that $\sigma = (\sigma_0/T) \exp - (H/kT)$, where σ is the conductivity at the absolute temperature T, σ_0 is the pre-exponential factor, H is the activation energy and k is the Boltzmann constant, H was evaluated as 0.74 eV and known to vary from 0.62 to 0.97 eV, depending on the powder synthesis and sintering profile, meaning that O^{2-} ions are the charge carriers [38].

5. Conclusions

$(CeO_2)_{0.8}(Sm_2O_3)_{0.2}$ ceramics sintered by applying an electric field without pressure (flash sintering) at 800 °C, 1000 °C and 1200 °C reached the same shrinkage level, which is higher than the level reached by conventional sintering at 1500 °C. The average grain size increased slightly for increasing flash sintering temperature and is smaller than in the sample sintered at 1500 °C. The samples flash sintered at 1000 °C and 1200 °C showed higher bulk ionic conductivity than the conventionally sintered sample. Flash sintering ceria-samaria solid electrolytes is a promising technique for densification at temperatures lower than the temperatures required in conventional sintering. Moreover, grain growth is inhibited and bulk conductivity is improved.

Author Contributions: Conceptualization, S.L.R. and E.N.S.M.; methodology, R.M. and S.L.R.; formal analysis, R.M., S.L.R. and S.G.M.C.; investigation, S.L.R., S.G.M.C., R.M. and E.N.S.M.; resources, R.M.; writing—original draft preparation, S.L.R.; writing—review and editing, R.M., S.L.R., S.G.M.C. and E.N.S.M.; supervision, R.M.; project administration, R.M.; funding acquisition, R.M. and E.N.S.M.

Funding: This research was funded by the Brazilian Agencies: CNEN, CNPq (Procs. 302357/2018-1 and 305889/2018-4), FAPESP (Proc. 2013/07296-2) and FAPESP-Shell (Proc. 2017/11937-4).

Acknowledgments: SLR had a CNPq post-doc scholarship (Proc. 150101/2017-1). SGMC has a FAPESP-Shell post-doc position. RM is grateful to Federal University of ABC for the Senior Visiting Researcher fellowship. To Dr. AM Figueiredo Neto, Institute of Physics, University of S. Paulo, Brazil, for making available the impedance analyzer.

Conflicts of Interest: The authors declare no conflict of interest.

References

1. Cologna, M.; Rashkova, B.; Raj, R. Flash Sintering of nanograin zirconia in < 5 s at 850 °C. *J. Am. Ceram. Soc.* **2010**, *93*, 3556–3559.
2. Yu, M.; Grasso, S.; Mckinnon, R.; Saunders, T.; Reece, M.J. Review of flash sintering: Materials, mechanisms and modelling. *Adv. Appl. Ceram.* **2017**, *116*, 24–60. [CrossRef]

3. Dancer, C.E.J. Flash sintering of ceramic materials. *Res. Express* **2016**, *3*, 1–25. [CrossRef]
4. Muccillo, R.; Muccillo, E.N.S. Electric field assisted sintering of electroceramics and in situ analysis by impedance spectroscopy. *J. Electroceram.* **2016**, *38*, 24–42. [CrossRef]
5. Guillon, O.; Elsässer, C.; Gutfleisch, O.; Janek, F.; Korte-Kerzel, S.; Raabe, D.; Volkert, C.A. Manipulation of matter by electric and magnetic fields: Toward novel synthesis and processing routes of inorganic materials. *Mater. Today* **2018**, *21*, 527–536. [CrossRef]
6. Biesuz, M.; Sglavo, V.M. Flash sintering of ceramics. *J. Eur. Ceram. Soc.* **2019**, *39*, 115–143. [CrossRef]
7. Yang, D.; Conrad, H. Enhanced sintering rate of zirconia (3Y-TZP) by application of a small AC electric field. *Scr. Mater.* **2010**, *63*, 328–331. [CrossRef]
8. Cologna, M.; Prette, A.L.G.; Raj, R. Flash-sintering of cubic yttria-stabilized zirconia at 750 degrees C for possible use in SOFC manufacturing. *J. Am. Ceram. Soc.* **2011**, *94*, 316–319. [CrossRef]
9. Muccillo, R.; Kleitz, M.; Muccillo, E.N.S. Flash grain welding in yttria stabilized zirconia. *J. Eur. Ceram. Soc.* **2011**, *31*, 1517–1521. [CrossRef]
10. Raj, R. Joule heating during flash sintering. *J. Eur. Ceram. Soc.* **2012**, *32*, 2293–2301. [CrossRef]
11. Muccillo, R.; Muccillo, E.N.S. An experimental setup for shrinkage evaluation during electric field-assisted flash sintering: Application to yttria-stabilized zirconia. *J. Eur. Ceram. Soc.* **2013**, *33*, 515–520. [CrossRef]
12. Downs, J.A.; Sglavo, V.M. Electric field assisted sintering of cubic zirconia at 390 °C. *J. Am. Ceram. Soc.* **2013**, *96*, 1342–1344. [CrossRef]
13. Francis, J.S.C.; Raj, R. Influence of the field and the current limit on flash sintering at isothermal furnace temperatures. *J. Am. Ceram. Soc.* **2013**, *96*, 2754–2758. [CrossRef]
14. M'Peko, J.C.; Francis, J.S.C.; Raj, R. Impedance spectroscopy and dielectric properties of flash versus conventionally sintered yttria-doped zirconia electroceramics viewed at the microstructural level. *J. Am. Ceram. Soc.* **2013**, *96*, 3760–3767. [CrossRef]
15. Muccillo, R.; Muccillo, E.N.S. Shrinkage control of yttria-stabilized zirconia during ac electric field-assisted sintering. *J. Eur. Ceram. Soc.* **2014**, *34*, 3871–3877. [CrossRef]
16. Todd, R.I.; Zapata-Solvas, E.; Bonilla, R.S.; Sneddon, T.; Wilshaw, P.R. Electrical characteristics of flash sintering: Thermal runaway of Joule heating. *J. Eur. Ceram. Soc.* **2015**, *35*, 1865–1877. [CrossRef]
17. Da Silva, J.G.P.; Lebrun, J.M.; Al-Qureshi, H.A.; Janssen, R.; Raj, R. Temperature Distributions During flash sintering of 8% yttria-stabilized zirconia. *J. Am. Ceram. Soc.* **2015**, *98*, 3525–3528. [CrossRef]
18. Dong, Y.H.; Chen, I.W. Onset criterion for flash sintering. *J. Am. Ceram. Soc.* **2015**, *98*, 3624–3627. [CrossRef]
19. Du, Y.X.; Stevenson, A.J.; Vernat, D.; Diaz, M.; Marinha, D. Estimating Joule heating and ionic conductivity during flash sintering of 8YSZ. *J. Eur. Ceram. Soc.* **2016**, *36*, 749–759. [CrossRef]
20. Jha, S.K.; Terauds, K.; Lebrun, J.M.; Raj, R. Beyond flash sintering in 3 mol % yttria-stabilized zirconia. *J. Ceram. Soc. Jpn.* **2016**, *124*, 283–288. [CrossRef]
21. Qin, W.; Yun, J.; Thron, A.M.; van Benthem, K. Temperature gradient and microstructure evolution in AC flash sintering of 3 mol% yttria-stabilized zirconia. *Mater. Manufact. Proc.* **2017**, *32*, 549–556. [CrossRef]
22. Carvalho, S.G.M.; Muccillo, E.N.S.; Muccillo, R. AC Electric field assisted pressureless sintering zirconia: 3 mol% yttria solid electrolyte. *Phys. Status Solidi A* **2018**, *215*, 1700647. [CrossRef]
23. Biesuz, M.; Sglavo, V.M. Microstructural temperature gradient-driven diffusion: Possible densification mechanism for flash sintering of zirconia? *Ceram. Int.* **2019**, *45*, 1227–1236. [CrossRef]
24. Campos, J.V.; Lavagnini, I.R.; de Souza, R.V.; Ferreira, J.A.; Pallone, E.M.D.A. Development of an instrumented and automated flash sintering setup for enhanced process monitoring and parameter control. *J. Eur. Ceram. Soc.* **2019**, *39*, 531–538. [CrossRef]
25. Carvalho, S.G.M.; Muccillo, E.N.S.; Muccillo, R. Electrical Behavior and Microstructural Features of Electric Field-Assisted and Conventionally Sintered 3 mol % Yttria-Stabilized Zirconia. *Ceramics* **2018**, *1*, 3–12. [CrossRef]
26. Bannister, M. *Science and Technology of Zirconia V*; Badwal, S.P.S., Bannister, M.J., Hannink, R.H.J., Eds.; CRC Press: Boca Raton, FL, USA, 1993.
27. Hao, X.; Liu, Y.; Wang, Z.; Qiao, J.; Sun, K. A novel sintering method to obtain fully dense gadolinia doped ceria by applying a direct current. *J. Power Sources* **2012**, *210*, 86–91. [CrossRef]
28. Jiang, T.Z.; Wang, Z.H.; Zhang, J.; Hao, X.M.; Rooney, D.; Liu, Y.; Sun, W.; Qiao, J.S.; Sun, K.N. Understanding the flash sintering of rare-earth-doped ceria for solid oxide fuel cell. *J. Am. Ceram. Soc.* **2015**, *98*, 1717–1723. [CrossRef]

29. Biesuz, M.; Dell'Agli, G.; Spiridigliozi, L.; Ferone, C.; Sglavo, V.M. Conventional and field-assisted sintering of nanosized Gd-doped ceria sinthesized by co-precipitation. *Ceram. Int.* **2016**, *42*, 11766–11771. [CrossRef]
30. Valdebenito, J.U.; Akbari-Fakhrabadi, A.; Viswanathan, M.R. Effect of flash sintering on microstructure of $Ce_{0.9}Gd_{0.1}O_{1.95}$ electrolyte fabricated by tape-casting. *Mater. Lett.* **2017**, *209*, 291–294. [CrossRef]
31. Spiridigliosi, L.; Biesuz, M.; Dell'Agli, G.; Di Bartolomeo, E.; Zurlo, F.; Sglavo, V.M. Microstructural and electrical investigation of flash-sintered Gd/Sm-doped ceria. *J. Mater. Sci.* **2017**, *52*, 7479–7488. [CrossRef]
32. Li, J.; Guan, L.L.; Zhang, W.; Luo, M.; Song, J.L.; Song, X.W.; An, S.L. Sintering behavior of samarium doped ceria under DC electrical field. *Ceram. Int.* **2018**, *44*, 2470–2477. [CrossRef]
33. Jha, S.K.; Charalambous, H.; Wang, H.; Phuah, X.L.; Mead, C.; Okasinski, J.; Wang, H.; Tsakalakos, T. In-situ observation of oxygen mobility and abnormal lattice expansion in ceria during flash sintering. *Ceram. Int.* **2018**, *44*, 15362–15369. [CrossRef]
34. Vendrell, X.; West, A.R. Induced p-type semi-conductivity in yttria-stabilised zirconia. *J. Am. Ceram. Soc.* **2019**. [CrossRef]
35. Samarium Doped Ceria (20% Sm)–Nanopowder. Available online: https://fuelcellmaterials.com/products/powders/electrolyte-powders/samarium-doped-ceria-20-sm-nanopowder/ (accessed on 4 April 2019).
36. Kleitz, M.; Kennedy, J.H. Resolution of multicomponent impedance diagrams. In *Fast Ion Transport in Solids*; Mundy, J.N., Shenoy, G.K., Vashishta, P., Eds.; Elsevier: North Holland, The Netherlands, 1979; pp. 185–188.
37. Barsoukov, E.; Macdonald, J.R. *Impedance Spectroscopy, Theory, Experiment, and Applications*; Wiley-Interscience: Hoboken, NJ, USA, 2005.
38. Ding, D.; Liu, B.; Gong, M.; Liu, X.; Xia, C. Electrical properties of samaria-doped ceria electrolytes from highly active powders. *Electrochim. Acta* **2010**, *55*, 4529–4535. [CrossRef]